JOURNAL OF GEOPHYSICAL RESEARCH, VOL. 114, C08009, doi:10.1029/2008JC004792, 2009

Low efficiency of nutrient translocation for enhancing oceanic uptake of carbon dioxide

Andrew Yool,[1] John G. Shepherd,[1] Harry L. Bryden,[1] and Andreas Oschlies[2]

Received 29 February 2008; revised 8 April 2009; accepted 28 May 2009; published 21 August 2009.

[1] Anthropogenic emissions of carbon dioxide (CO_2) are steadily increasing the concentration of this greenhouse gas in the Earth's atmosphere. The possible long-term consequences of this elevated concentration have led to proposals for a number of large-scale geoengineering schemes that aim to enhance or augment natural sinks for CO_2. One such scheme proposes deploying a large number of floating "pipes" in the ocean that act to translocate nutrient-rich seawater from below the mixed layer to the ocean's surface: the nutrient supplied should enhance the growth of phytoplankton and consequently the export of organic carbon to the deep ocean via the biological pump. Here we examine the practical consequences of this scheme in a global ocean general circulation model that includes a nitrogen-based ecosystem and the biogeochemical cycle of carbon. While primary production is generally enhanced by the modeled pipes, as expected, the effect on the uptake of CO_2 from the atmosphere is much smaller, may be negative, and shows considerable spatiotemporal variability.

Citation: Yool, A., J. G. Shepherd, H. L. Bryden, and A. Oschlies (2009), Low efficiency of nutrient translocation for enhancing oceanic uptake of carbon dioxide, *J. Geophys. Res.*, *114*, C08009, doi:10.1029/2008JC004792.

1. Introduction

[2] Since the beginning of the Industrial Revolution, atmospheric CO_2 concentrations have been rising in response to human activities including fossil fuel combustion, deforestation, land use changes and cement production. However, the rise in atmospheric CO_2 has not paralleled anthropogenic emissions. A significant fraction of the CO_2 released to the atmosphere has been removed to reservoirs on the land and, particularly, in the ocean [*Revelle and Seuss*, 1957]. While there is still uncertainty in the role that these reservoirs will play in the near future [*Friedlingstein et al.*, 2006], in the long term (1000 years or more) most anthropogenic CO_2 will be absorbed by the ocean through dissolution enhanced by processes including calcium carbonate compensation and silicate weathering [*Archer*, 2005]. In terms of the Earth's climate, since anthropogenic CO_2 that is transferred to land or ocean sinks cannot cause global warming there is continuing interest in establishing (and enhancing) the capacity and rate of uptake of these reservoirs.

[3] This long-term oceanic fate of much of the CO_2 released by human activities, as well as the role of the ocean in modulating past climate change, has led to several proposals for geoengineering schemes which aim to accelerate the transfer of CO_2 to the ocean. Some of these have focused on the direct transfer of sequestered CO_2 (in liquid or solid form) to the deep ocean [e.g., *Brewer et al.*, 1999]. Others have proposed to exploit the ocean's so-called biological pump to increase the rate of CO_2 absorption by the ocean [e.g., *Cooper et al.*, 1996]. The biological pump consists of a suite of ecological processes that act to transport organic and inorganic carbon from the surface ocean to the deep ocean [*Raven and Falkowski*, 1999; *Sarmiento and Gruber*, 2006]. The pump is ultimately driven by the primary production of phytoplankton in the ocean's euphotic zone, and nutrient availability strongly regulates their growth. Consequently, enhancing primary production and the biological pump may act to draw CO_2 into the ocean at a faster rate than at present.

[4] A number of different methods have been proposed for accelerating the biological pump. The most widely known involves the application of the micronutrient iron to so-called high-nutrient, low-chlorophyll (HNLC) regions of the world ocean [*Martin*, 1990; *Martin et al.*, 1990]. Deficiency of iron in these regions is believed to restrict primary production, leading to the accumulation of macronutrients (e.g., nitrate, phosphate, and silicic acid). Application of iron to these regions has been demonstrated to trigger phytoplankton blooms and an increase in the air-to-sea flux of CO_2 [e.g., *Cooper et al.*, 1996]. However, only a fraction of the world ocean is HNLC, the majority instead exhibits the reverse problem: a deficit of macronutrients. This deficit is an inevitable consequence of faster consumption than recycling of nutrients, gravitational sinking (export) of particulate material and relatively low rates for physical mechanisms that mix nutrients from deep water back to the surface. One proposal for enhancing primary production in these oligotrophic regions is to supply macronutrients directly, through the injection of either artificially synthe-

[1] National Oceanography Centre, Southampton, Southampton, UK.
[2] Leibniz Institute of Marine Sciences at University of Kiel (IFM-GEOMAR), Kiel, Germany.

0148-0227/09/2008JC004792$09.00

sized ammonia or nutrient-rich effluent such as agricultural waste [*Shoji and Jones*, 2001].

[5] A recently proposed method focuses instead on exploiting the strong gradient of macronutrients with depth, and argues that nutrient-rich water from depth could be translocated to the ocean's surface where it can fuel primary production and enhance the biological pump [*Lovelock and Rapley*, 2007]. It is envisaged that this translocation is achieved through the use of pipes incorporating one-way valves that exploit wave energy to "pump" up water from beneath the euphotic zone and the seasonal nutricline [*Liu et al.*, 1999; *Kithil*, 2006; *Kenyon*, 2007]. Such a scheme could work in any area where primary production is limited by macronutrient concentration (i.e., unlike iron fertilization schemes which are limited to HNLC regions). An alternative scheme, known as the "perpetual salt fountain" [*Stommel et al.*, 1956], exploits gradients in density, temperature conductance and salinity nonconductance to drive similar pipes [*Maruyama et al.*, 2004; *Tsubaki et al.*, 2007]. Typical dimensions suggested for the pipes are a 10 m diameter and a length of 100–200 m [*Lovelock and Rapley*, 2007]. *Kithil* [2006] describes a prototype of 1 m diameter and a length of 1000 m, which would allow the pipes to successfully straddle the nutricline in most oligotrophic regions. Networks of these pipes, either free floating or tethered to the seafloor, would then be distributed across regions with low surface nutrients to increase the activity of the biological pump in locations where its role is normally limited by macronutrients under natural conditions. Such pipe systems are already under commercial development, and it is proposed that they may have additional benefits such as enhancing mariculture [*Liu et al.*, 1999], hurricane abatement through surface ocean cooling [*Kithil*, 2006] and power generation from subsurface wave energy [*Isaacs et al.*, 1976] or ocean thermal energy conversion [*Takahashi*, 2000].

[6] This paper considers this pipe geoengineering scheme and explores its efficacy through the use of a specially configured ocean global ocean general circulation model (GCM). The GCM includes an idealized representation of such a pipe scheme, together with a carbon cycle coupled to a nitrogen-based plankton ecosystem model. The scheme is examined from the perspective of first primary production, then export production, and finally the air-to-sea exchange of CO_2, with analysis of both the large-scale effects and the spatiotemporal patterns of efficacy for each of these.

2. Model Description

2.1. Physical Model

[7] The work here makes use of the Ocean Circulation and Climate Advanced Modeling (OCCAM) physical model, a global, medium-resolution, primitive equation, finite difference ocean general circulation model (a 1/4° high-resolution version is described by *Marsh et al.* [2005]). OCCAM's vertical resolution is 66 levels (with thickness ranging from 5 m at the surface to 200 m at the abyssal seafloor), with a horizontal resolution of typically 1° (~100 km). OCCAM's prognostic variables are temperature, salinity, velocity and free surface height.

[8] OCCAM includes an elastic-viscous-plastic sea ice scheme, a *K* profile parameterization (KPP) mixed layer and the Gent-McWilliams eddy parameterization. Advection is fourth-order accurate (a modified Split-QUICK scheme), and the model employs fractional bottom grid boxes to allow a more realistic representation of bathymetry. OCCAM is time integrated using a forward leapfrog scheme with a time step of 1 h. Surface fluxes of heat, freshwater and momentum are not specified directly, but are calculated using empirical formulae and NCEP-derived basic atmospheric boundary layer quantities [*Large and Yeager*, 2004]. Local day length is calculated and used in conjunction with daily averaged irradiance to reconstruct a realistic diel cycle. To compensate for deficiencies in the freshwater flux balance, surface salinity is relaxed toward monthly observations.

[9] Simulations are forced at the surface with high-resolution spatial and temporal data for the period January 1958 to December 2004 inclusive. Spin-up cycles made repeated use of this period (i.e., upon reaching 2004, the model state was "recycled" to 1958). Although this approach tends to warm the ocean, in practice this trend is small [*Yool and Sinha*, 2006].

2.2. Biogeochemical Model

[10] Biogeochemical cycles of nitrogen, carbon, oxygen and alkalinity are embedded within OCCAM. These cycles are driven primarily by an existing nitrogen-based nutrient-phytoplankton-zooplankton-detritus (NPZD) model [*Oschlies*, 2001] that was tuned with particular emphasis on upper ocean nutrient supply [*Oschlies*, 2002] and coupled to the other elemental cycles [*Anderson and Pondaven*, 2003; *Sinha and Yool*, 2006; *Yool and Sinha*, 2006]. The adaptations necessary for this coupling include: $C:N:O_2$ Redfield relationships for phytoplankton and zooplankton [*Anderson*, 1995; *Palmer and Totterdell*, 2001]; a separate tracer variable for detrital carbon [*Anderson and Pondaven*, 2003]; a simplified scheme for biogenic calcium carbonate production and dissolution [*Najjar and Orr*, 1999; *Najjar et al.*, 2007]; and subroutines to calculate the air-sea exchange of CO_2 and oxygen [*Orr et al.*, 1999; *Najjar and Orr*, 1999]. The model also incorporates a variable detrital sinking velocity [*Schmittner et al.*, 2005]. The model does not include any representation of other nutrient cycles such as phosphorus, silicon or iron.

[11] The resulting model comprises eight tracer variables that are entirely passive and distributed throughout the model domain. A unified set of equations governs the biogeochemical tendencies throughout the water column, and these are described in the auxiliary material.[1] Figure S1 shows a diagrammatic representation of the model components and the interactions that link them. Minor variants of this ecosystem model have previously been used within the OCCAM GCM in unrelated studies [*Yool et al.*, 2007; *Glessmer et al.*, 2008].

2.3. Ocean Pipes

[12] The low resolution of the ocean GCM used in this work precludes a physically realistic representation of the ocean pipes scheme. The pipes proposed are of order 1–10 m in diameter, but model grid cells are of order 100 km on a side. Instead, the model is adapted such that ocean tracers are

[1] Auxiliary materials are available in the HTML. doi:10.1029/2008JC004792.

aphysically translocated between a selected deep model level and a near-surface level (model level 2, at ~5–10 m). This upward transport is balanced by compensating downward transports of ocean tracers between each of the intervening model levels. Figure S2 shows a diagrammatic representation of these vertical transports. Since the tracers are inescapably distributed throughout a grid cell, this representation corresponds to the limiting case where the pipe effluent is rapidly mixed laterally before significant sinking occurs. Only dissolved tracers are translocated, and particulate tracers such as phytoplankton, zooplankton and detritus are unaffected by the pipes (i.e., it is assumed that some degree of filtration operates at a pipe's mouth). In the equations below, X_k represents an ocean tracer on level k, z_k is the layer thickness of level k, n is the level from which the ocean pipe draws seawater and w^* is the spatially averaged upward translocation rate (note that simple upstream differencing is used for these quasi-advective terms).

$$\frac{\partial X_2}{\partial t} = + \underbrace{\left[\frac{w^* . X_n}{z_2}\right]}_{\text{pipe transport} \uparrow} - \underbrace{\left[\frac{w^* . X_2}{z_2}\right]}_{\text{compensation} \rightarrow} \quad (1)$$

$$\frac{\partial X_k}{\partial t} = + \underbrace{\left[\frac{w^* . X_{k-1}}{z_k}\right]}_{\rightarrow \text{compensation}} - \underbrace{\left[\frac{w^* . X_k}{z_k}\right]}_{\text{compensation} \rightarrow} \quad (2)$$

$$\frac{\partial X_n}{\partial t} = + \underbrace{\left[\frac{w^* . X_{n-1}}{z_n}\right]}_{\rightarrow \text{compensation}} - \underbrace{\left[\frac{w^* . X_n}{z_n}\right]}_{\text{pipe transport} \uparrow} . \quad (3)$$

[13] In the simulations described here, w^* was set to a value of 2 cm d^{-1}, approximately double the canonical background rate of ocean ventilation [*Broecker and Peng*, 1982]. This relatively high rate (which corresponds to about 70 Sv of upwelling globally) was chosen so that the simulated effect of the pipes was of a similar order of magnitude to background biogeochemical processes. In separate simulations the depth of the pipe "mouth" was set to 200 m (level 21), 500 m (level 29) and 1000 m (level 36). To explore the consequences of the pipes scheme for the widest range of ocean conditions, the simulated pipes were applied globally, wherever water column depth exceeded 1000 m.

[14] Because of the difference in scale between ocean pipes and OCCAM grid cells, the configuration of the model described above approximates a case in which each grid cell contains a large number of evenly distributed ocean pipes that, when integrated across the cell, transport water upward at a rate of w^*. It is envisaged that the pipes would actually transport water at a significantly higher rate, but that an average rate of 2 cm d^{-1} would apply at the scale of the grid cell. For similar reasons, the operation of the ocean pipes is crudely represented as a simple vertical displacement of tracer concentration since the physical process of water transport by the pipes cannot properly be resolved in a global GCM.

[15] To avoid disrupting the physical dynamics of OCCAM, initial simulations only translocated passive tracers. In reality, ocean pipes would actually translocate deep water of higher density to the surface (though heat diffusion across the pipe walls may partially offset this), with consequences for water column stability. To examine these effects, sensitivity simulations have been performed that include potential temperature and salinity. In these cases, both of these active tracers were translocated in exactly the same manner as the passive tracers, with the subsequent dynamical adjustments to the density field being modeled normally. As already noted, OCCAM includes a relaxation term for salinity, and this term was switched off during these sensitivity analyses to prevent it from interfering with the translocated salinity. An additional control simulation was performed to check the model's performance in the absence of relaxation.

2.4. Simulations

[16] Simulations were initialized from restart states of an existing simulation of the recent historical period, which doubles here as a control. This extant simulation was initialized from rest with tracer fields from the World Ocean Atlas 2001 (temperature, salinity, nitrate, and oxygen [*Conkright et al.*, 2002]) and GLODAP (carbon and alkalinity [*Key et al.*, 2004]) climatologies. After an initial spin-up cycle (using surface forcing data from 1958 to 2004; see above), the simulation underwent three further forcing cycles during which the time history of atmospheric CO_2 from 1864 to 2004 was applied. Figure 1 shows comparisons of oceanic primary production and the air-sea CO_2 flux between OCCAM and observations. While the simulation has deficiencies (see Figure 1 caption) we judged it to be adequate as the initial state for examining the ocean pipes scheme.

[17] Although there are as yet no ongoing ocean pipe schemes in operation and their use is proposed for future amelioration of anthropogenic CO_2 emissions, for simplicity simulations performed here focused on their application to the recent past. Experiment simulations were initialized from the restart state at the end of 1994, and the effect of the pipes was simulated for a 10 year period to the end of 2004. The simulations were otherwise performed in an identical manner to that of the control from which they were initialized. During the initial experiments which involved only the translocation of passive tracers, the physical state of OCCAM remained identical to that in the control simulation.

3. Results

[18] The aim of the ocean pipes geoengineering scheme is to utilize the biological pump to increase the ocean's uptake of CO_2 by enhancing first primary production and then export production and, thus, air-sea flux. For this reason, the model analysis focuses here on these three biogeochemical fluxes of carbon.

[19] Figure 2 (top) shows a time series of annually integrated global primary production for the period 1992 to 2004. The control simulation runs for this full period, with the ocean pipes experiments running from the beginning of 1995 onward. Primary production in the pipes

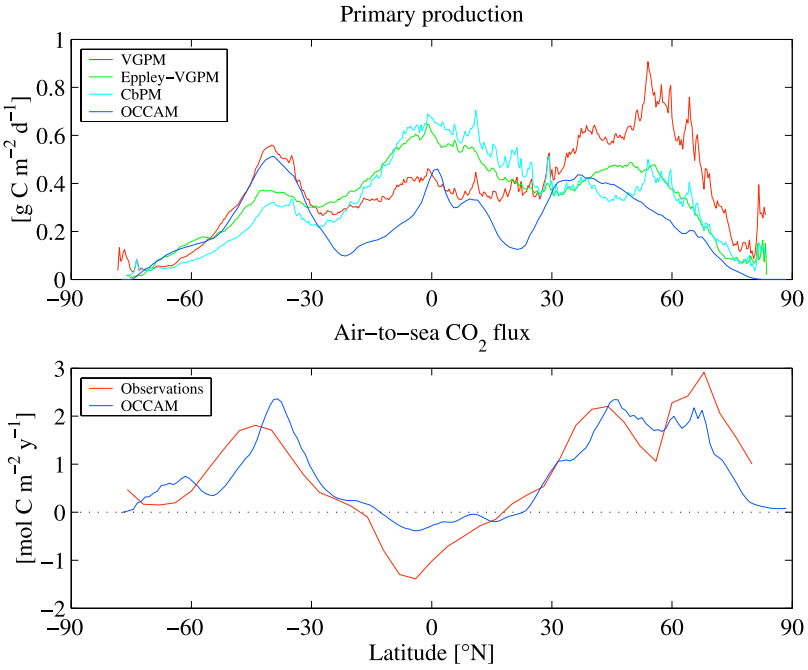

Figure 1. Comparison of zonally averaged observational and model fields of (top) primary production and (bottom) air-sea CO_2 flux. Primary production observations are derived by applying the Vertically Generalized Production Model (VGPM) [*Behrenfeld and Falkowski*, 1997], Eppley-VGPM [*Carr et al.*, 2006], and Carbon-based Production Model (CbPM) [*Westberry et al.*, 2008] productivity models to Sea-viewing Wide Field-of-view Sensor (SeaWiFS) fields of surface chlorophyll for the period 2003 to 2004. Air-sea CO_2 flux observations are those estimated by *Takahashi et al.* [2002] for the standardized year 1995. The corresponding model outputs are the averages of these fields for the matching periods. In terms of primary production, the model shows the greatest discrepancy with observations in the subtropics. In these regions, the model typically underestimates production in the gyre centers and shows a more pronounced "equatorial stripe" of higher productivity. The model is generally in better agreement at higher latitudes, although it underestimates productivity in the Northern Hemisphere (especially with respect to the VGPM model). The model shows greater agreement with observational air-sea CO_2 flux and generally captures its zonal trends. The greatest discrepancy in this field lies in the equatorial region, where the model underestimates outgassing of CO_2 to the atmosphere.

experiments responds immediately, and saturates within around 4 years. Not surprisingly, given the vertical distribution of nutrients, primary production responds increasingly strongly to deeper ocean pipes, with the 1000 m pipes elevating primary production by almost 50%. The shallower pipes show more modest increases with slightly more than 30% for 500 m pipes and around 10% for 200 m pipes. The relatively short duration of the experimental simulations prevents strong conclusions about the long-term behavior of primary production, but both the 500 m and, especially, the 200 m pipe experiments appear to show gradual declines in the elevated production that they initially cause.

[20] Tracing the fate of this enhanced primary production down the water column, Figure 2 (middle) shows the changes in the annually integrated global export flux (=sinking flux) of detrital material at 200 m depth (i.e., below the euphotic zone). The changes over time here closely mirror those of primary production with a relatively rapid response to the activation of ocean pipes followed by saturation within approximately 4 years. However, the magnitude of the responses observed are somewhat different, with export increasing by a greater percentage than primary production. For instance, the 1000 m pipes show export flux increases beyond that of primary production at almost 60% during the simulated period, with the 500 m pipes similarly elevated at 40%. With the 200 m pipes, export production is only marginally enhanced and follows primary production in showing a gradual decline in the increased production.

[21] Finally, Figure 2 (bottom) shows the changes in the annually integrated air-sea flux of CO_2. In contrast to the previous carbon fluxes, the behavior of the air-sea flux in response to the ocean pipes is more complex. Whereas the pipes led to systematic and substantial increases in primary and export production, here the CO_2 flux from the atmosphere to the ocean is actually decreased at first as high CO_2 seawater from depth is brought to the surface decreasing the air-sea flux. To illustrate this, Figure 3 shows the time evolution of surface dissolved inorganic carbon (DIC) properties, while Figure 4 shows how the pipes change the vertical profile of DIC between their first and final years of operation. This outgassing is ultimately reversed in all three experimental simulations, but this requires several years and is not a simple function of pipe depth. Initially, the magnitude of the fall in CO_2 uptake is related to pipe depth, with deeper pipes having progressively greater

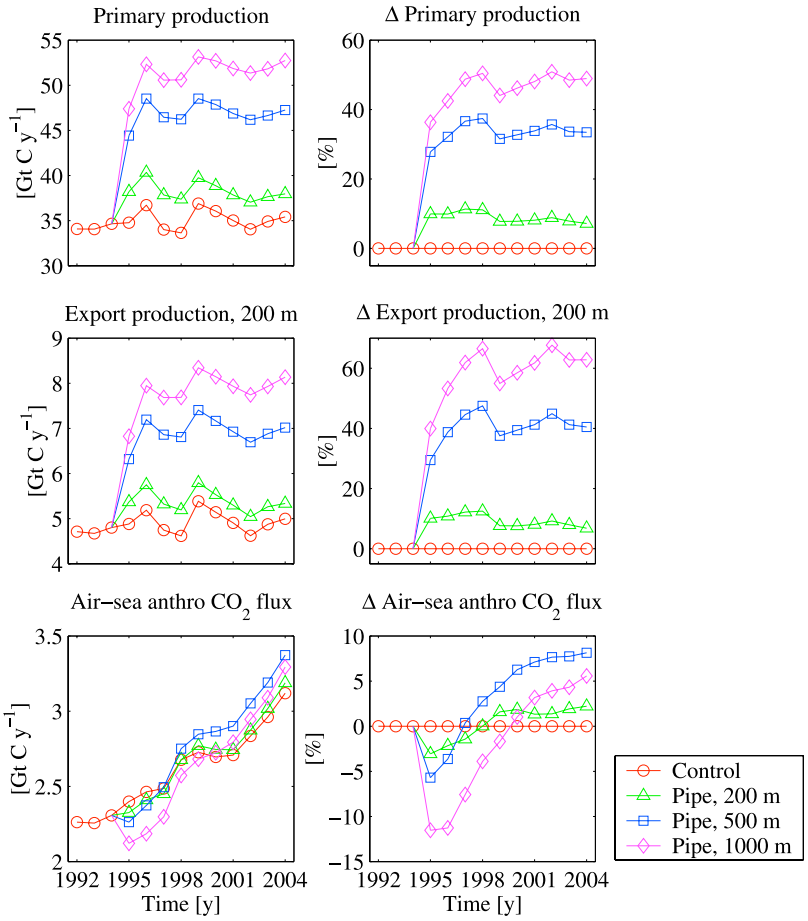

Figure 2. Annual time series of globally integrated (top) primary production (Gt C a^{-1}), (middle) export production at 200 m (Gt C a^{-1}), and (bottom) air-sea CO_2 flux (Gt C a^{-1}) for the simulated period 1992 to 2004 inclusive. Experiments including simulated ocean pipes begin in 1995. Figure 2 (left) shows the integrated fluxes for all four simulations, while Figure 2 (right) shows the change in fluxes (%) between the experimental and control simulations.

decreases. However, in the timing of the break-even point, where the pipes switch from decreasing the flux to increasing it, the 500 m pipes reach this point first, with the 200 m then the 1000 m pipes following afterward. While the ocean pipes therefore do ultimately lead to a (proportionally small) enhancement of the air-sea flux of CO_2, the 10 year duration of the simulations here is insufficient for the 1000 m experiment to show a net increase in oceanic CO_2 storage: by the end of 2004 (10 years) the simulation has taken up 0.3 gigatons (Gt) C less than the control simulation.

[22] Table 1 summarizes these carbon fluxes and the differences between the experiments and the control for the full experimental period. Export production is resolved at four depth horizons to determine trends in the fate of sinking material. This shows that while export is enhanced more by the pipes than is primary production, the magnitude of this increase declines with depth. The simulated pipes are only located in water deeper than 1000 m, and some of this apparent decline in export flux is probably due to the horizontal transport of sinking detritus into neighboring, shallower water columns.

[23] While the pipes operate uniformly across the world ocean in these simulations, the distribution of changes induced in the biogeochemical fluxes of carbon are non-uniform and show strong regional variations. Figure 5 shows the absolute differences in primary production, export production and air-sea CO_2 flux between the experimental simulations and the control, integrated over the final year (2004; the intention here is to show output away from unrepresentative initial transient behavior). Figure S3 shows the corresponding relative changes in fluxes for comparison. Primary production and export production are strongly coupled, with changes (broadly increases in production) confined almost exclusively to tropical and subtropical regions (approximately 40°S to 40°N). With the exception of the equatorial upwelling regions of the eastern Atlantic and Pacific basins, where surface nutrient concentrations are already elevated by natural upward transport, pipe-induced changes in primary production and export fluxes are exclusively positive. The 200 m and, to a lesser extent, 500 m pipe experiments show slight declines in primary production and export in these upwelling regions only. These declines are driven by slight falls in nutrient availability, despite the pipes. The strongest positive responses are found within the centers of the subtropical gyres, where these fluxes are considerably enhanced over the background oligotrophic conditions typical for these regions. By contrast, the magnitudes of these fluxes in the productive

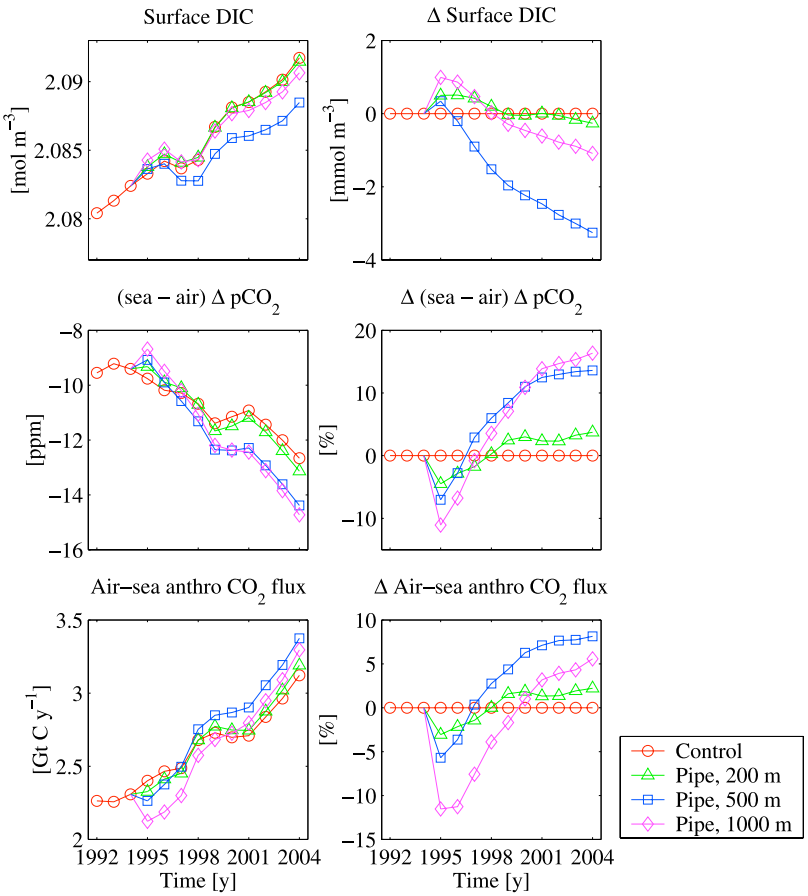

Figure 3. Annual time series of globally integrated (top) surface DIC (mmol m^{-3}), (middle) surface (sea minus air) ΔpCO_2 (ppm), and (bottom) air-sea CO_2 flux (Gt C a^{-1}) for the simulated period 1992 to 2004 inclusive. Experiments including simulated ocean pipes begin in 1995. Figure 3 (left) shows the integrated properties for all four simulations, while Figure 3 (right) shows their changes between the experimental and control simulations.

temperate latitudes (approximately 40° to 60°) are almost completely unchanged.

[24] However, the air-sea CO_2 flux shows much greater heterogeneity in its behavior. While, like primary production, the tropical and subtropical regions still respond most positively to ocean pipes, the response is proportionally far less, and temperate and polar latitudes now also show changes in the magnitude of the air-sea flux. This response is strongest in the Southern Ocean and, most significantly, the North Pacific Ocean. In these regions, the translocation of DIC from depth to the surface actually leads to less CO_2 being absorbed. This is a minor effect in the case of shallow translocation, but becomes increasingly significant with the deeper ocean pipes. In the most extreme case, a 10° zonal band of the North Pacific (45°N to 55°N) is transformed from a sink (0.6 mol C m^{-2} a^{-1}) of CO_2 into a source (−0.3 mol C m^{-2} a^{-1}) through the action of 1000 m pipes. However, in most regions where there is a negative response to the pipes, this is a marginal decline in the uptake of CO_2 by the end of the simulation. In some regions, such as the subpolar North Atlantic Ocean, there is a marginal increase in air-sea flux in spite of the absence of any biological response to the pipes.

[25] Table 2 summarizes the changes in carbon fluxes between the experiments and the control for the final year. These are also integrated for only those regions of the world ocean where the CO_2 flux is enhanced (mask 1). This markedly increases the fractional gain of the ocean pipes (particularly 200 m and 1000 m), although it decreases the gain in primary production for all three experiments since some regions increase organic carbon production while decreasing uptake of atmospheric CO_2. However, since it is not entirely straightforward a priori to identify areas where the CO_2 uptake is enhanced, the fluxes are also integrated for the tropical ocean region (30°S to 30°N; mask 2). This latter region brackets that where the experiments broadly overlap in terms of biological response, and is intended to reflect a real-world deployment of pipes where the precise behavior of individual ocean regions is uncertain. While this more prosaic approach is unsurprisingly less successful than a retrospective selection of beneficial deployment areas, relative to global integrals it still finds moderate returns in the case of 200 m (0.069 → 0.045 Gt C a^{-1}) and 500 m pipes (0.254 → 0.214 Gt C a^{-1}), and good returns with 1000 m pipes (0.174 → 0.343 Gt C a^{-1}). To illustrate the temporal behavior of these regional trends, Figure 6 repeats Figure 2 but splits the time series into tropical and extratropical regions. With respect to primary production and export, the extratropics respond to the pipes in a similar manner to the tropics, but with much smaller relative

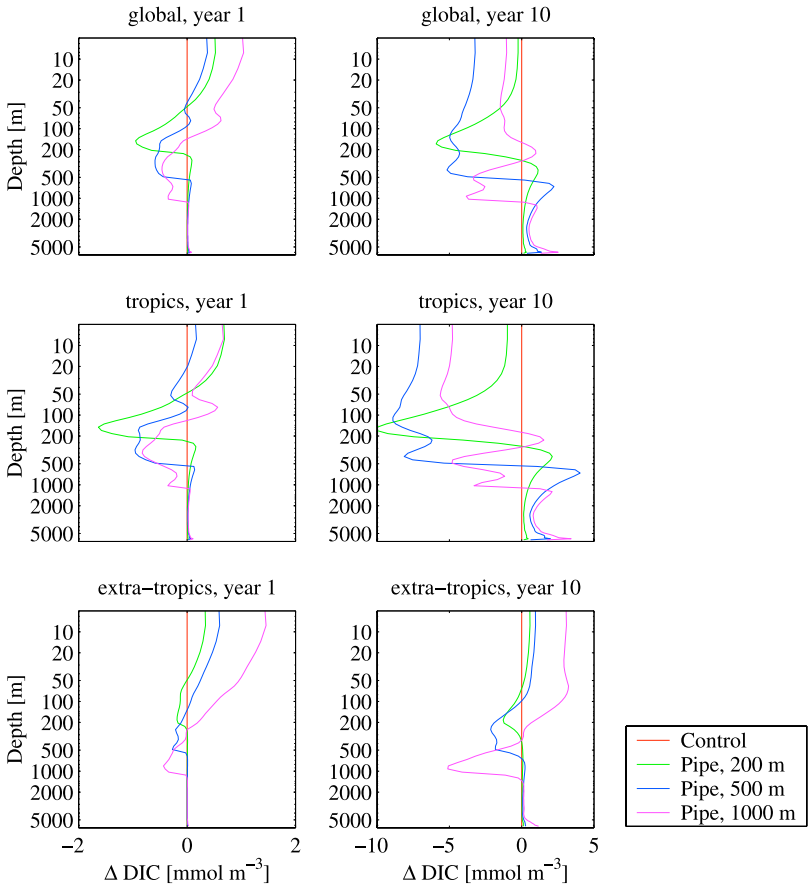

Figure 4. Changes in the vertical distributions of DIC between (left) year 1 and (right) year 10, (top) integrated globally, (middle) for the tropics (30°S to 30°N), and (bottom) for the extratropical regions (30–90°). The changes in distributions are shown relative to the control simulation. All concentrations are in mmol m^{-3}.

changes. As Table 2 already highlights, the tropics and extratropics show very different behavior in terms of air-sea CO_2 fluxes. The tropics show generally higher uptake by the ocean, while the extratropics show only slight increases, or even large decreases (1000 m pipes).

[26] Table 2 also estimates "pipe efficiency" of the experiments by relating gains in the uptake of CO_2 to those of primary production. In general, pipe efficiency is typically less than 3%. This seemingly low efficiency should be viewed within the context that most organic carbon is remineralized in the upper ocean (more than 95% by 1000 m in the control simulation). Integrated globally, efficiency falls as the pipes increase in length, although deeper pipes generate larger fluxes of carbon for the same volume of water translocated. While an efficiency of 7.3% is recorded when only those 200 m pipes that enhanced CO_2 uptake are considered, this uptake represents less than a 5% increase over the control.

[27] Finally, Table 3 presents summarized results from the active tracer sensitivity experiments. A second control is shown since these simulations do not include salinity relaxation. Although, relative to the default control, circulation is slightly weakened in this latter control simulation, it did not show significant changes (although the simulations had a relatively short duration). In terms of the biogeochemical fluxes, at the large scale the patterns of

Table 1. Biogeochemical Fluxes of Carbon Averaged for the Experimental Period 1995 to 2004 Inclusive[a]

		Pipes		
Field	Control	200 m	500 m	1000 m
Primary production	35.143	38.289 (9.0%)	46.902 (33.5%)	51.458 (46.4%)
Export flux, 100 m	7.428	8.126 (9.4%)	10.308 (38.8%)	11.565 (55.7%)
Export flux, 200 m	4.934	5.389 (9.2%)	6.926 (40.4%)	7.836 (58.8%)
Export flux, 500 m	2.986	3.229 (8.2%)	4.043 (35.4%)	4.539 (52.0%)
Export flux, 1000 m	1.715	1.847 (7.7%)	2.284 (33.2%)	2.552 (48.8%)
Air-sea CO_2 flux	2.707	2.720 (0.5%)	2.810 (3.8%)	2.670 (−1.4%)

[a]Flux values are in Gt C a^{-1}. The fluxes are globally integrated, and the values from pipe simulations are accompanied by the percentage difference from those of the control simulation.

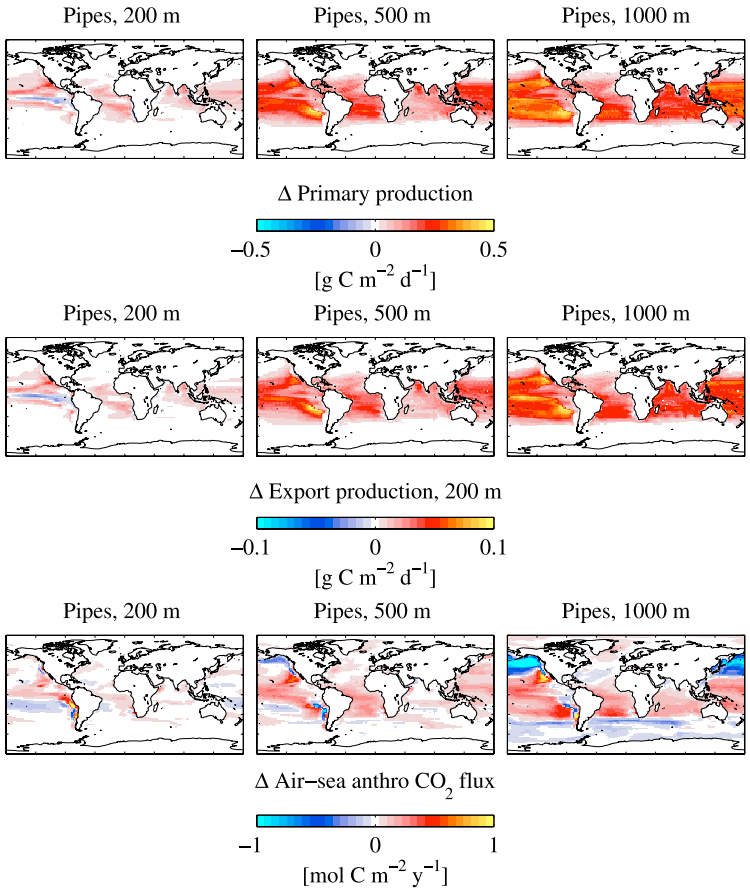

Figure 5. Annual average fields of the difference in (top) primary production (g C m^{-2} d^{-1}), (middle) export production at 200 m (g C m^{-2} d^{-1}), and (bottom) air-sea CO_2 flux (mol C m^{-2} a^{-1}) between the control simulation field and each of the experimental simulations. All model output used is from the final simulated year, 2004.

change caused by the simulated ocean pipes remain very similar: primary production and export show increases in the tropics, while air-sea CO_2 fluxes respond positively in the tropics but negatively at higher latitudes. However, at the smaller scale the changes in local fluxes are both more exaggerated and noticeably more patchy. In the case of primary production, where high latitudes were essentially unaffected by the pipes, localized regions of productivity gains and losses now occur. Nonetheless, as Table 3 indicates, the results are qualitatively comparable to those of the earlier simulations.

4. Discussion

[28] Ocean pipes represent one in a series of geoengineering schemes that aim to alter the Earth system to offset or compensate for changes to the planetary energy balance driven by anthropogenic emissions of CO_2. Unlike other schemes that propose to actively fertilize the ocean through the introduction of micronutrients [cf. *Buesseler et al.*, 2008] or macronutrients [*Shoji and Jones*, 2001], ocean pipes fertilize through the redistribution of existing macronutrients. Nonetheless, these schemes aim to enhance the uptake of CO_2 by the ocean through inducements made to the autotrophic drivers of the biological pump. As such, obvious biological side effects include changes to biodiversity as oligotrophic communities are replaced by mesotrophic ones [cf. *Grob et al.*, 2007], and accelerated ocean acidification as CO_2 is drawn into the ocean faster [cf. *Orr et al.*, 2005]. The ecosystem model used here is too simplified to allow analysis of such effects, and this work instead focuses on a more basic question: do the pipes work?

[29] The simulations performed here find that, after an initial decrease in the uptake of CO_2, the modeled pipes do ultimately enhance the ocean's role as a sink for CO_2. The correlation with enhanced biological productivity is generally strong, though production responds and saturates more quickly in response to the pipes, and there is considerable variability in the relationship (e.g., regions where CO_2 uptake and production are inversely related). Broadly speaking, production and CO_2 uptake is enhanced most in low latitudes and the subtropical gyres, with ocean pipes in temperate and polar regions causing only small enhancement of ocean productivity and frequently turning the ocean into a source of CO_2 for the atmosphere. Figure 7 illustrates the relationship between the trophic status of surface waters and the resulting changes in CO_2 uptake. While anthropogenic CO_2 uptake is driven exclusively by dissolution of CO_2 at the surface in the model and is greatest in cooler mesotrophic regions, it is enhanced most by the pipes through the operation of the biological pump in warm oligotrophic regions. Figure 7 (bottom) shows the changes

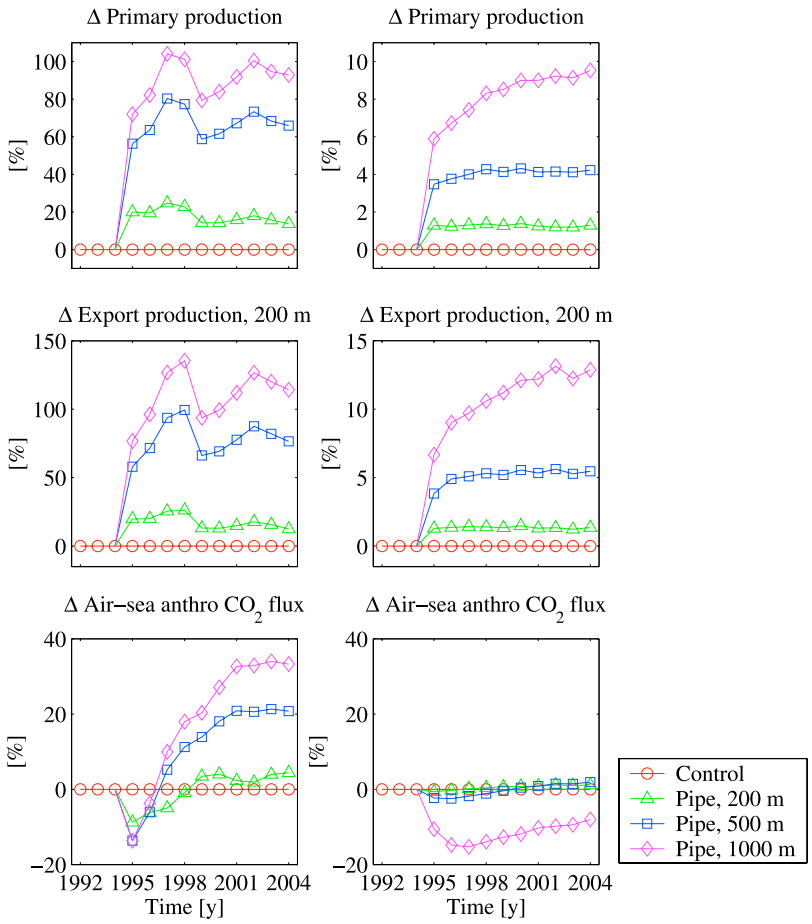

Figure 6. As in Figure 2 except showing the relative changes (%) in (top) primary production, (middle) export production at 200 m, and (bottom) air-sea CO_2 flux for the (left) tropical (30°S to 30°N) and (right) extratropical regions. Note the different vertical scales for primary production and export between the two regions.

in surface nutrient concentrations that result from the pipes. Although the largest absolute increases occur in nutrient-replete mesotrophic regions, oligotrophic regions experience much larger relative increases.

[30] In quantitative terms, however, ocean pipes are less successful. Since most organic carbon is remineralized within the upper ocean, a generally low efficiency is to be expected. As reported in Table 2, the model simulations find

Table 2. Biogeochemical Fluxes of Carbon Integrated for the Final Simulation Year and With a Range of Ocean Masks Applied[a]

		Pipes					
		200 m		500 m		1000 m	
Field	Control Total	Δ	Percent	Δ	Percent	Δ	Percent
Primary production	35.507	2.555	7.2	11.876	33.5	17.389	49.0
Mask 1		1.577	4.4	10.475	29.5	15.359	43.3
Mask 2		2.314	6.5	11.086	31.2	15.607	44.0
Export flux, 200 m	5.009	0.341	6.8	2.027	40.5	3.146	62.8
Mask 1		0.221	4.4	1.816	36.3	2.779	55.5
Mask 2		0.307	6.1	1.888	37.7	2.819	56.3
Air-sea CO_2 flux	3.128	0.069	2.2	0.254	8.1	0.174	5.6
Mask 1		0.115	3.7	0.298	9.5	0.415	13.3
Mask 2		0.045	1.4	0.214	6.9	0.343	11.0
Field		200 m		500 m		1000 m	
Pipe efficiency		2.7		2.1		1.0	
Mask 1		7.3		2.8		2.7	
Mask 2		1.9		1.9		2.2	

[a]Pipe efficiency is the fraction of the increase in air-sea CO_2 flux relative to that of primary production. The first row for each flux shows the globally integrated value for the control simulation together with the differences (actual and percentage) for each of the three ocean pipes experiments. The second row (mask 1) includes only those regions where the CO_2 flux into the ocean is enhanced. The third row (mask 2) includes only the region 30°S to 30°N. Fluxe values are in Gt C a^{-1}.

Table 3. Globally Averaged Physical Properties and Integrated Biogeochemical Fluxes of Carbon for the Final Simulation Year of the Active Tracer Sensitivity Simulations[a]

			Active Tracer Sensitivity Simulations			
Field	Units	Default Control Total	Control Total	200 m Δ	500 m Δ	1000 m Δ
Surface temperature	°C	17.492	17.476	17.468	17.422	17.359
Surface salinity	psu	34.751	34.769	34.770	34.724	34.696
Mixed layer depth	m	55.495	52.556	54.516	57.090	60.027
Primary production	Gt C a^{-1}	35.507	35.338	4.752	14.886	19.831
Export flux, 200 m	Gt C a^{-1}	5.009	5.050	0.787	2.599	3.592
Air-sea CO_2 flux	Gt C a^{-1}	3.128	2.974	0.158	0.307	0.055

[a]The default control simulation is shown alongside the corresponding active tracer control simulation for this sensitivity analysis. The carbon fluxes shown for the pipe experiments are the differences due to the control total for the sensitivity simulation. Here psu indicates practical salinity units.

an efficiency of around 2–3% in terms of carbon fixed to air-sea uptake. Oceanic uptake of CO_2, primarily driven by the solubility pump, is currently estimated at around 2 Gt C a^{-1} (1995 value [*Takahashi et al.*, 2002]), while productivity is estimated at around 40–50 Gt C a^{-1} [*Behrenfeld and Falkowski*, 1997]. The low efficiency is therefore consistent with that of the inadvertently perturbed natural system. Extrapolating model estimates from the 1000 m pipes simulations (and confining the pipes to the tropics; occupying 173 × 10^6 km^2 and achieving 2.2% efficiency), for the ocean to uptake an extra 1 Gt C a^{-1}, primary production would need to be enhanced by about 45 Gt C a^{-1}, i.e., doubled. This would require a much greater quantity of upwelling (117 Sv) than we assumed, and the number of pipes required to achieve this (1 m diameter, capable of pumping 13 × 10^3 m^3 d^{-1} [*Kithil*, 2006]) would be 776 million. The number of pipes required will, of course, depend upon the technology employed and its pumping efficiency. For example, *Liu et al.* [1999] estimate a higher rate of 54 × 10^3 m^3 d^{-1} for their prototype, which suggests that fewer pipes would be needed (189 million). It should be noted that, when integrated over the global ocean, the seemingly low upward flow rate of 0.02 m d^{-1} in our simulations translates to approximately 70 Sv, which represents the activity of approximately 465 million ocean pipes [*Kithil*, 2006].

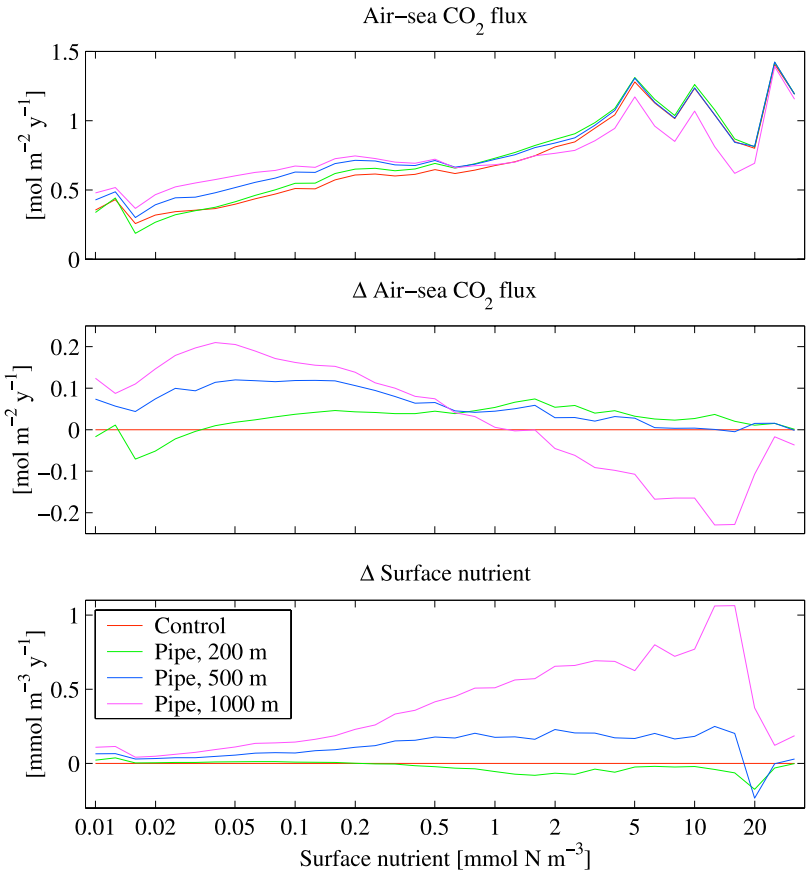

Figure 7. (top) Average CO_2 flux, (middle) the change in this flux, and (bottom) the change in surface nutrient concentration expressed against surface nutrient concentration from the control simulation. All model output used is from the final simulated year, 2004. The output is plotted on a logarithmic scale and indicates a logarithmic response of the air-sea CO_2 flux to surface nutrients.

[31] There are a number of caveats to the work reported here. First, this study has only explored three idealized situations in which the whole world ocean is "plumbed in" with identical pipes of three different lengths. While the results from using pipes of different lengths generally suggest that longer is better (since nutrient concentrations broadly increase with depth), this is not universally true. For instance, in the case of 1000 m pipes, this length results in both the greatest outgassing as well as the greatest uptake of anthropogenic CO_2. As Figure 5 shows, there are some regions where 500 m pipes are more successful than those that reach 1000 m into the ocean. These include areas of the Northwestern Pacific (30°N to 60°N), the Northwestern Atlantic (20°N to 40°N) and the Indian sector of the Southern Ocean (30°S to 60°S). In part this is due to whether the ocean pipes successfully access reservoirs of "preformed nutrients" [*Sarmiento and Gruber*, 2006]. Nutrients reach the deep ocean from the surface either as the result of remineralization of organic material, or through physical processes such as advection or mixing. The latter pathway distinguishes preformed nutrients that, unlike remineralized nutrients, are not accompanied by carbon. As such, upwelling these does not bring this associated carbon that would offset efforts to draw CO_2 from the atmosphere (although net outgassing may still occur because of surface warming). Preformed and remineralized nutrients can be identified through apparent oxygen utilization, and the length of the ocean pipes, like their geographical distribution, could be tailored to maximize the use of preformed nutrients.

[32] Second, the simulations performed have been of very limited duration. In the case of primary (and export) production, the ocean appears to reach a quasi-equilibrium by the end of the simulations (although the results from the 200 m simulation suggest that the gains in productivity may yet decline). However, this is not the case for the air-sea flux of CO_2, where an initial negative response gives way to a positive response which is still on the path toward quasi-equilibrium at the end of the simulations (this is true even where analysis is restricted to only those regions where pipes enhance uptake). Operated over a longer period of time, the pipes may also change nutrient distributions sufficiently to alter natural routes of their resupply to the surface ocean. The application of lower-resolution models capable of much longer integrations (century to millennial) may elucidate any such long-term trends (e.g., intermediate complexity models such as GENIE [*Lenton et al.*, 2007]).

[33] Third, because of the relatively low spatial resolution of the model physics (extremely low relative to the dimensions of proposed ocean pipes), the vertical translocation of tracers is modeled implicitly and in an idealized manner. This is particularly aphysical in the case of temperature and salinity, which are moved with no consideration for seawater density or in-pipe effects (e.g., heat diffusion). In addition, the tracers are instantly and unavoidably redistributed throughout each grid cell, so our simulations represent the limiting case where lateral mixing overwhelms the vertical sinking to be expected when dense water is translocated to the surface. Such sinking would partially nullify the effectiveness of the pipes in translocating nutrients, so our results represent an upper limit to their efficacy. While no current or foreseeable global models can improve on this situation because of the large gap between grid scale and pipe diameter, localized studies at much higher resolution may permit some exploration of these aspects (e.g., regional models such as HOPS [*Popova et al.*, 2007]). Furthermore, models based on unstructured grids that self-organize to improve resolution around small-scale features, such as those around the mouth of an ocean pipe, may be able to provide a more complete understanding of local hydrography [e.g., see *Piggott et al.*, 2008]. Such models may also be useful to address a further uncertainty, namely, the medium- and longer-term spatial structure of the recirculation loops driven by the pipes (here assumed to be localized; equations (1)–(3)), and hence the source of the water which replenishes that upwelled from the depth horizon to which the pipes extend.

[34] Finally, the modeled biogeochemistry omits much of the detail of real ecosystems, and may not respond realistically to the nutrients supplied by the pipes. For example, the model does not include a representation of the ocean's silicon cycle and the diatoms [*Yool and Tyrrell*, 2003]. This particular group of phytoplankton are believed to play a disproportionately important role in the biological pump [*Dugdale and Wilkerson*, 1998; *Armstrong et al.*, 2002], but their regulating nutrient, silicic acid, is regenerated on a longer length scale and deeper in the water column than other macronutrients. Consequently, while the ocean pipes may readily supply nitrate and phosphate in a Redfield ratio, silicic acid may be deficient and the resulting nutrient mixture may favor a plankton community that drives a weaker biological pump. Similarly, the model does not include the micronutrient iron, which is known to play an important role in HNLC regions [*Martin et al.*, 1990; *Boyd et al.*, 2007] and for which there are separate geoengineering schemes [*Lampitt et al.*, 2008]. Although HNLC regions may not respond to the addition of further macronutrients, the transport of iron from deeper waters by the pipes may lead to a significant response. Other changes in community structure may even have wider consequences; for instance, shifts in the abundance of phytoplankton that produce dimethyl sulphide could even impact on climate [*Charlson et al.*, 1987; *Gunson et al.*, 2006]. This study's model only coarsely resolves the biogeochemical cycles of nitrogen and carbon, but the use of models with more detailed representations of the marine ecosystem [cf. *Hood et al.*, 2006] may capture potentially significant interactions such as these.

[35] Notwithstanding the uncertainty introduced by these caveats, the primary quantitative hurdle that the ocean pipes must overcome if they are to significantly enhance oceanic uptake of CO_2 is the rapid remineralization of organic carbon in near-surface waters. Unless production shifts the plankton community structure to favor exporting groups such as silicifiers or calcifiers, or is stimulated sufficiently to decrease water column remineralization through anoxia, the resulting low efficiency is inescapable, and likely to prohibit the exploitation of this scheme on economic grounds alone. The possible side effects for the oceanic biota of this (and other ocean fertilization schemes [*Lampitt et al.*, 2008]) are a further and very important consideration given the massive enhancement of natural productivity required to achieve globally significant increase in CO_2 uptake by the ocean.

[36] Nevertheless, the deficiencies of this study suggest several future avenues for progress that merit further inves-

tigation. (1) What are the optimal pipe distribution and length parameters? (2) What are the longer-term (century-scale) consequences of pipe-enhanced vertical transport? (3) What are the local, small-scale consequences for ocean physics (e.g., sea surface temperature and mixed layer depth)? (4) How does the community structure of plankton ecosystems respond to changes in nutrient supply and stoichiometry (e.g., N:P:Si:Fe)? Because of modeling deficiencies in terms of physical scale and ecological complexity, the latter two questions may best be answered by direct experiments, potentially by small-scale trials in the tropical ocean [cf. *Karl and Letelier*, 2008], analogous to existing trials of iron fertilization [*Boyd et al.*, 2007]. Nonetheless, all four questions can be addressed fruitfully through the application of existing or elaborated models, bearing in mind the limitations that these have.

[37] In summary, while these simulations represent a simple and short-term analysis of a specific proposal, they illustrate why all such geoengineering schemes need to be carefully examined before they are promoted as promising or worthy of investment. In addition, they illustrate what the ecologist Garrett Hardin referred to as the first law of ecology: "We can never do merely one thing" [*Hardin*, 1985].

5. Conclusions

[38] (1) Primary production and the air-sea flux of CO_2 can be enhanced by the deployment of ocean pipes. (2) Changes in primary production are almost always positive, but substantial changes are confined to low latitudes and the subtropical gyres. (3) Changes in the air-sea flux of CO_2 can be both positive and negative, and some regions of the world ocean can be turned into sources of CO_2 to the atmosphere. (4) Since almost all organic carbon is remineralized in the upper ocean, increases in CO_2 uptake are substantially smaller than increases in productivity (primary and export). (5) Integrated over beneficial regions, increases in primary production of 100% typically result in a 2–3% increase in the air-sea flux of CO_2 (carbon for carbon). (6) On the basis of this efficiency and estimated pump efficiency, enhancing the ocean's uptake of CO_2 by 1 Gt C a^{-1} would require approximately 0.8 billion pumps (of 1 m diameter) to be deployed.

[39] **Acknowledgments.** The authors would like to thank Bablu Sinha, George Nurser, Beverly de Cuevas, and Andrew Coward for technical assistance with OCCAM; Débora Iglesias-Rodríguez, Richard Lampitt, Katya Popova, and other NOCS colleagues for discussions of oceanic geoengineering; Robert O'Malley (Oregon State University) for providing observational primary production estimates; and Ruth Roberts (formerly Impossible Pictures, United Kingdom) for information concerning some practicalities of ocean pipes. The authors are grateful to James Lovelock and two anonymous referees for comments that helped to improve the paper. A.Y. is funded on a U.K. National Environment Research Council (NERC) standard grant (NE/C00387X/1). The authors declare that they have no competing interests.

References

Anderson, L. A. (1995), On the hydrogen and oxygen content of marine phytoplankton, *Deep Sea Res., Part I*, *42*, 1675–1680.

Anderson, T. R., and P. Pondaven (2003), Non-redfield carbon and nitrogen cycling in the Sargasso Sea: Pelagic imbalances and export flux, *Deep Sea Res., Part I*, *50*, 573–591.

Archer, D. (2005), Fate of fossil fuel CO_2 in geologic time, *J. Geophys. Res.*, *110*, C09S05, doi:10.1029/2004JC002625.

Armstrong, R. A., C. Lee, J. I. Hedges, S. Honjo, and S. G. Wakeham (2002), A new, mechanistic model for organic carbon fluxes in the ocean: Based on the quantitative association of POC with ballast minerals, *Deep Sea Res., Part II*, *49*, 219–236.

Behrenfeld, M. J., and P. G. Falkowski (1997), Photosynthetic rates derived from satellite-based chlorophyll concentration, *Limnol. Oceanogr.*, *42*, 1–20.

Boyd, P. W., et al. (2007), Mesoscale iron enrichment experiments 1993–2005: Synthesis and future directions, *Science*, *315*, 612–617.

Brewer, P. G., et al. (1999), Direct experiments on the ocean disposal of fossil fuel CO_2, *Science*, *284*, 943–945.

Broecker, W. S., and T.-H. Peng (1982), *Tracers in the Sea*, Lamont-Doherty Geol. Obs., Palisades, N. Y.

Buesseler, K. O., et al. (2008), Environment: Ocean iron fertilization — Moving forward in a sea of uncertainty, *Science*, *319*, 162–162.

Carr, M.-E., et al. (2006), A comparison of global estimates of marine primary production from ocean color, *Deep Sea Res., Part II*, *53*, 741–770.

Charlson, R. J., J. E. Lovelock, M. O. Andreae, and S. G. Warren (1987), Oceanic phytoplankton, atmospheric sulphur, cloud albedo and climate, *Nature*, *326*, 655–661.

Conkright, M. E., et al. (2002), *World Ocean Database 2001*, vol. 1, *Introduction*, *NOAA Atlas NESDIS*, vol. 42, edited by S. Levitus, Silver Spring, Md.

Cooper, D. J., A. J. Watson, and P. D. Nightingale (1996), Large decrease in ocean-surface CO_2 fugacity in response to in situ iron fertilization, *Nature*, *383*, 511–513.

Dugdale, R. C., and F. P. Wilkerson (1998), Silicate regulation of new production in the equatorial Pacific upwelling, *Nature*, *391*, 270–273.

Friedlingstein, P., et al. (2006), Climate-carbon cycle feedback analysis: Results from the C^4MIP model intercomparison, *J. Clim.*, *19*, 3337–3353.

Glessmer, M. S., A. Oschlies, and A. Yool (2008), Simulated impact of double-diffusive mixing on physical and biogeochemical upper ocean properties, *J. Geophys. Res.*, *113*, C08029, doi:10.1029/2007JC004455.

Grob, C., et al. (2007), Picoplankton abundance and biomass across the South Pacific Ocean along latitude 32.5°S, *Mar. Ecol. Prog. Ser.*, *332*, 53–62.

Gunson, J. R., S. A. Spall, T. R. Anderson, A. Jones, I. J. Totterdell, and M. J. Woodage (2006), Climate sensitivity to ocean dimethylsulphide emissions, *Geophys. Res. Lett.*, *33*, L07701, doi:10.1029/2005GL024982.

Hardin, G. (1985), *Filters Against Folly*, Viking, New York.

Hood, R. R., et al. (2006), Pelagic functional group modeling: Progress, challenges and prospects, *Deep Sea Res., Part II*, *53*, 459–512.

Isaacs, J. D., D. Castel, and G. L. Wick (1976), Utilization of the energy in ocean waves, *Ocean Eng.*, *3*, 175–187.

Karl, D. M., and R. M. Letelier (2008), Nitrogen fixation–enhanced carbon sequestration in low nitrate, low chlorophyll seascapes, *Mar. Ecol. Prog. Ser.*, *364*, 257–268.

Kenyon, K. E. (2007), Upwelling by a wave pump, *J. Oceanogr.*, *63*, 327–331.

Key, R. M., A. Kozyr, C. L. Sabine, K. Lee, R. Wanninkhof, J. L. Bullister, R. A. Feely, F. J. Millero, C. Mordy, and T.-H. Peng (2004), A global ocean carbon climatology: Results from Global Data Analysis Project (GLODAP), *Global Biogeochem. Cycles*, *18*, GB4031, doi:10.1029/2004GB002247.

Kithil, P. (2006), A device to control sea surface temperature and effects on hurricane strength, *Eos Trans. AGU*, *87*(36), Ocean Sci. Meet. Suppl., Abstract OS25C-10.

Lampitt, R. S., et al. (2008), Ocean fertilization: A potential means of geoengineering?, *Philos. Trans. R. Soc. A*, *366*, 3919–3945, doi:10.1098/rsta.2008.0139.

Large, W., and S. Yeager (2004), Diurnal to decadal global forcing for ocean and sea-ice models: The data sets and flux climatologies, *NCAR Tech. Note NCAR/TN-460+STR*, Clim. and Global Dyn. Div., Natl. Cent. for Atmos. Res., Boulder, Colo.

Lenton, T. M., et al. (2007), Effects of atmospheric dynamics and ocean resolution on bi-stability of the thermohaline circulation examined using the Grid Enabled Integrated Earth system modelling (GENIE) framework, *Clim. Dyn.*, *29*, 591–613.

Liu, C. C. K., J. J. Dai, H. S. Lin, and F. Guo (1999), Hydrodynamic performance of wave-driven artificial upwelling device, *J. Eng. Mech.*, *125*, 728–732.

Lovelock, J. E., and C. G. Rapley (2007), Ocean pipes could help the Earth to cure itself, *Nature*, *447*, 403.

Marsh, R., B. A. de Cuevas, A. C. Coward, H. L. Bryden, and M. Alvarez (2005), Thermohaline circulation at three key sections of the North Atlantic over 1985–2002, *Geophys. Res. Lett.*, *32*, L10604, doi:10.1029/2004GL022281.

Martin, J. (1990), Glacial-interglacial CO_2 change: The iron hypothesis, *Paleoceanography*, *5*, 1–13.

Martin, J. H., R. M. Gordon, and S. E. Fitzwater (1990), Iron in Antarctic waters, *Nature*, *349*, 156–158.

Maruyama, S., K. Tsubaki, K. Taira, and S. Sakai (2004), Artificial upwelling of deep seawater using the perpetual salt fountain for cultivation of ocean desert, *J. Oceanogr.*, *60*, 563–568.

Najjar, R. G., and J. C. Orr (1999), Biotic-HOWTO, internal OCMIP report, 15 pp., Lab. des Sci. du Clim. et l'Environ., Gif-sur-Yvette, France. (Available at www.ipsl.jussieu.fr/OCMIP/).

Najjar, R. G., et al. (2007), Impact of circulation on export production, dissolved organic matter, and dissolved oxygen in the ocean: Results from phase II of the Ocean Carbon-cycle Model Intercomparison Project (OCMIP–2), *Global Biogeochem. Cycles*, *21*, GB3007, doi:10.1029/2006GB002857.

Orr, J., R. Najjar, C. Sabine, and F. Joos (1999), Abiotic-HOWTO, internal OCMIP report, 29 pp., Lab. des Sci. du Clim. et l'Environ., Gif-sur-Yvette, France. (Available at www.ipsl.jussieu.fr/OCMIP/).

Orr, J. C., et al. (2005), Anthropogenic ocean acidification over the twenty-first century and its impact on calcifying organisms, *Nature*, *437*, 681–686.

Oschlies, A. (2001), Model-derived estimates of new production: New results point toward lower values, *Deep Sea Res., Part II*, *48*, 2173–2197.

Oschlies, A. (2002), Nutrient supply to the surface waters of the North Atlantic: A model study, *J. Geophys. Res.*, *107*(C5), 3046, doi:10.1029/2000JC000275.

Palmer, J. R., and I. J. Totterdell (2001), Production and export in a global ocean ecosystem model, *Deep Sea Res., Part I*, *48*, 1169–1198.

Piggott, M. D., G. J. Gorman, C. C. Pain, P. A. Allison, A. S. Candy, B. T. Martin, and M. R. Wells (2008), A new computational framework for multi-scale ocean modelling based on adapting unstructured meshes, *Int. J. Numer. Methods Fluids*, *56*, 1003–1015.

Popova, E. E., R. T. Pollard, M. Lucas, H. J. Venables, and T. R. Anderson (2007), Real-time forecasting of ecosystem dynamics during the CROZEX experiment and the roles of light, iron, silicate, and circulation, *Deep Sea Res., Part II*, *54*, 1966–1988.

Raven, J. A., and P. G. Falkowski (1999), Oceanic sinks for atmospheric CO_2, *Plant Cell Environ.*, *22*, 741–755.

Revelle, R., and H. E. Seuss (1957), Carbon dioxide exchange between atmosphere and ocean and the question of an increase of atmospheric CO_2 during the past decades, *Tellus*, *9*, 18–27.

Sarmiento, J., and N. Gruber (2006), *Ocean Biogeochemical Dynamics*, Princeton Univ. Press, Princeton, N. J.

Schmittner, A., A. Oschlies, X. Giraud, M. Eby, and H. L. Simmons (2005), A global model of the marine ecosystem for long-term simulations: Sensitivity to ocean mixing, buoyancy forcing, particle sinking, and dissolved organic matter cycling, *Global Biogeochem. Cycles*, *19*, GB3004, doi:10.1029/2004GB002283.

Shoji, K., and I. S. F. Jones (2001), The costing of carbon credits from ocean nourishment plants, *Sci. Total Environ.*, *277*, 27–31.

Sinha, B., and A. Yool (2006), Extension of the OCCAM 1° ocean general circulation model to include the biogeochemical cycles of carbon and oxygen, part I: Technical description, *Res. Consult. Rep. 5*, 81 pp., Natl. Oceanogr. Cent., Southampton, U. K.

Stommel, H., A. B. Arons, and D. Blanchard (1956), An oceanographic curiosity: The perpetual salt fountain, *Deep Sea Res.*, *3*, 152–153.

Takahashi, M. M. (2000), *DOW: Deep Ocean Water as Our Next Natural Resource*, translated from Japanese by K. Kitazawa and P. Snowden, Terra Sci., Tokyo.

Takahashi, T., et al. (2002), Global sea-air CO_2 flux based on climatological surface ocean pCO_2, and seasonal biological and temperature effects, *Deep Sea Res., Part II*, *49*, 1601–1622.

Tsubaki, K., S. Maruyama, A. Komiya, and H. Mitsugashira (2007), Continuous measurement of an artificial upwelling of deep sea water induced by the perpetual salt fountain, *Deep Sea Res., Part I*, *54*, 75–84.

Westberry, T., M. J. Behrenfeld, D. A. Siegel, and E. Boss (2008), Carbon-based primary productivity modeling with vertically resolved photoacclimation, *Global Biogeochem. Cycles*, *22*, GB2024, doi:10.1029/2007GB003078.

Yool, A., and B. Sinha (2006), Extension of the OCCAM 1° ocean general circulation model to include the biogeochemical cycles of carbon and oxygen, part II: Initial experiments, *Res. Consult. Rep. 6*, 159 pp., Natl. Oceanogr. Cent., Southampton, U. K.

Yool, A., and T. Tyrrell (2003), Role of diatoms in regulating the ocean's silicon cycle, *Global Biogeochem. Cycles*, *17*(4), 1103, doi:10.1029/2002GB002018.

Yool, A., A. P. Martin, C. Fernández, and D. R. Clark (2007), The significance of nitrification for oceanic new production, *Nature*, *447*, 999–1002.

H. L. Bryden, J. G. Shepherd, and A. Yool, National Oceanography Centre, Southampton, European Way, Southampton SO14 3ZH, UK. (axy@noc.soton.ac.uk)

A. Oschlies, Leibniz Institute of Marine Sciences at University of Kiel (IFM-GEOMAR), Düsternbrooker Weg 20, D-24105 Kiel, Germany.